

Article

Superparamagnetic Nanocomposites Templated with Pyrazole-Containing Diblock Copolymers

Sanchita Biswas¹, Kevin D. Belfield^{1,*}, Ritesh K. Das², Siddhartha Ghosh² and Arthur F. Hebard²

- ¹ Department of Chemistry, University of Central Florida, P.O. Box 162366, Orlando, FL 32816, USA; E-Mail: sbiswas@lsu.edu
- ² Department of Physics, University of Florida, Gainesville, FL 32611, USA;
 E-Mails: rkdas@aps.anl.gov (R.K.D.); ghoshsi@phys.ufl.edu (S.G.); afh@phys.ufl.edu (A.F.H.)
- * Author to whom correspondence should be addressed; E-Mail: belfield@ucf.edu; Tel.: +1-407-823-1028; Fax: +1-407-823-2252.

Received: 19 March 2012; in revised form: 26 April 2012 / Accepted: 14 May 2012 / Published: 31 May 2012

Abstract: Monodisperse maghemite nanoparticles, templated in novel, well-defined pyrazole-containing norbornene-based block copolymers, provided a superparamagnetic nanocomposite with high saturation magnetization at room temperature under an applied magnetic field. The synthesis of the polymer nanocomposites and physical, morphological, and magnetic chracaterization of the nanocomposites are reported. Micelle-encapsulated superparamagnetic nanocomposites were generated for dispersal in aqueous medium. Their stability in water in the presence of a magnetic field was investigated as was their morphology and cell viability, strongly suggesting the potential of these superparamagnetic polymer-based nanocomposites in certain biomedical imaging and associated applications.

Keywords: block copolymer; polymeric nanocomposite; maghemite; ROMP; chelating ligand

1. Introduction

There has been great interest in magnetic nanoparticles for a number of biomedical applications, including medical diagnosis and imaging, magnetic separation, magnetic hyperthermia, and controlled drug delivery [1–7] as well as for biomimetic applications [8–10], such as magnetically controlled locomotion of artificial bacterial flagellar motors [11] and artificial muscles [12]. Magnetic resonance

imaging (MRI) is a powerful 3D technique for noninvasive imaging (deeper penetration) of anatomic and physicochemical details of tissue and blood flow and diagnosis of a number of diseases [13,14]. To improve MRI resolution and image quality several paramagnetic iron oxide nanoparticles, based on Fe₂O₃ and Fe₃O₄ [15,16], have been employed as negative contrast agents in clinical trials [1,17–21]. Among these, newly developed ultrasmall superparamagnetic iron oxide (USPIO) is, perhaps, the most promising because of its absence of magnetic hysteresis at ambient temperature, high magnetization change under applied magnetic field, tunability of sizes of the nanoparticles, non-toxicity, and rapid clearance from the organs [22–25]. USPIO enhances MRI images by decreasing the T₁- and T₂- relaxation behavior of the water molecules through interaction with the superparamagnetic iron oxide core, inducing signal increases in T₁-weighted images (T₁-w) and signal reduction in T₂-weighted-gradient-echo (T*₂-w) images [26–28]. Control of uniformity and stability of nano-sized particles given the tendency to reduce surface energy. Thus, strategies to prepare stable magnetic nanoparticle dispersions are of significant interest, e.g., via coating the nanoparticle surface with ligands that act to prevent agglomeration.

Ligands grafted to a polymer backbone offer a means to control stability as well as spatial behavior [29]. An iron-binding, anchoring ligand (siderophore) is present in one block of the diblock copolymer to chelate iron-oxide nanoparticles while the other block contains a steric stabilizing group which helps isolate the magnetic nanoparticles from each other and facilitate dispersion. Our previous success in formation of stable and well-dispersed maghemite (γ -Fe₂O₃)-polymer nanocomposites led to the design of more effective ligand systems through exploiting the chemistry of the oxirane group [30,31]. There are several natural iron-protein complexes that play an important role in a number of physiological processes, e.g., transferring [32,33], ferritin, and hemeproteins (e.g., hemoglobin, myoglobin, neuroglobin), where stable bonding between iron (III or II) core and protoporphrin IX and the imidazole group of the histidine protein residue forms. Here, we functionalized the oxirane with the 2,3-dimethylpyrazole group, a very close analog of imidazole, to study the chelation behavior with the iron-oxide nanoparticles for better stabilization compared to common chelating functional groups such as -COOH, -OH, -NH₂, phosphate. Ring opening metathesis polymerization (ROMP), a powerful and broadly applicable method compared to other controlled living polymerization techniques, was employed to synthesize highly functionalized block copolymers with low polydispersity to form superparamagnetic nanocomposite [7,34–36].

We present a strategy for the synthesis of a novel norbornene-based diblock copolymer, via ROMP of a functional monomer, and subsequent *in situ* generation and stabilization of maghemite nanoparticles to form superparamagnetic nanocomposites. The polynorbornene backbone was selected for its high thermal stability, optical transparency, low dielectric constant, and good mechanical properties [37]. In addition, functionalized norbornene-based monomers are readily polymerizable, which is thermodynamically favorable by releasing the strain in the monomer, by highly tolerant Grubbs catalysts into low polydispersity copolymers with readily tailored block ratios. The block copolymers design, contains "chelating groups" in one block to bind with the metal nanoparticles and "steric-stabilizing" block in another block to prevent agglomeration, was preferred for the nanocomposite generation. The anchoring group was synthesized by taking advantage of the versatility of oxirane ring-opening by the heterocycle pyrazole, creating a ligand to stabilize maghemite nanopaticles through strong coordination. The stable binding of this ligand system represents a

significant advance over our previously reported materials [23,24]. Well-defined novel diblock copolymers, containing 1:1 anchoring and steric stabilizing blocks, were characterized by NMR, gel permeation chromatography (GPC), thermogravimetric analysis (TGA), and differential scanning calorimetry (DSC). The ligand-stabilized organic-inorganic hybrid nanocomposites were prepared into self-assembled 1:1 block copolymer matrix *in situ* by a non-hydrolytic procedure using Fe(CO)₅ [31] and morphology and particle nature were characterized with TEM, Electron diffraction pattern, SEM and XRD. Magnetic measurements on the nanocomposite were performed using SQUID magnetometer demonstrates the typical superparamagnetic properties with better magnetization in presence of magnetic field.

For biomedical applications, biocompatibility along with aqueous dispersibility and stability of the superparamagnetic nanocomposites are essential. PluronicTM copolymers are well known in the pharmaceutical industry to improve the solubility of hydrophobic drugs [38] and to increase biocompatibility and blood circulation time [39,40]. Pluronic[™] F127 is a triblock polymer of poly(ethylene oxide)-poly(propylene-oxide)-poly(ethylene oxide) (PEO-PPO-PEO), consisting of 70 wt% PEO. Stabilization of several types of nanoparticles by Pluronic F127 was reported to maintain stable suspensions in a high ionic strength environment [41]. It is reported in literature that iron oxide nanoparticles were stabilized in water by phase transfer from an organic medium while maintaining its inherent magnetic properties for drug delivery purposes [42,43]. Pluronic F127 also provides antifouling properties to prevent aggregation and protein adsorption along with recognition by reticuloendothelial system (RES) [44]. But Pluronic F127 is a stabilizer of intermediate strength for nanoparticles. Here, Pluronic F127 was chosen as a carrier to encapsulate the stable, new pyrazole block copolymer-stabilized nanocomposites, to provide an aqueous dispersibility and biocompatibility [45]. The magnetic nanocomposite was encapsulated with F127 to provide water dispersability, subsequent determination of aqueous stability was examined by TEM. To assess cytotoxicity of the resulting micelle-encapsulated magnetic nanocomposites, a cell viability assay was performed with Hela cells.

2. Experimental

2.1. General

2.1.1. Materials

Bis(tricyclohexylphosphine)-benzylideneruthenium dichloride Grubbs' second generation catalyst, 3,5-dimethylpyrazole, Fe(CO)₅ (99.9%), and trimethylamine *N*-oxide (98%), DMF were purchased from Aldrich and used as received. CH₂Cl₂ and CHCl₃ were dried over CaCl₂ and distilled. Tetrahydrofuran (THF) was distilled over sodium and benzophenone under N₂ before use. All catalyst solutions were prepared in a glovebox. Pluoronic F127 (M_w ~12600) prill was purchased from BASF. Promega CellTiter 96[®] AQueous One Solution Reagent was purchased from Fisher. Hela cells were purchased from ATCC (America Type Culture Collection, Manssas, VA, USA). All cells were incubated in Minimum Essential Media (MEM, Invitrogen, Carlsbad, CA, USA), supplemented with 10% fetal bovine serum (FBS, Atlanta Biologicals, Lawrenceville, GA, USA) and incubated at 37 °C in a 95% humidified atmosphere containing 5% CO₂.

2.1.2. Characterization

¹H NMR and ¹³C NMR spectra were acquired on a Varian spectrometer at 500 and 125 MHz, respectively, using CDCl₃ as the solvent for all monomers and polymers. Elemental analysis was performed at Atlantic Microlab, Inc., Norcross, GA. All FTIR studies were done using a Perkin-Elmer Spectrum One FTIR spectrometer from 4000 to 500 cm⁻¹. Gel permeation chromatography (GPC) was conducted with a Waters 2414 refractive index detector, Waters 2996 photodiode array, and Waters 1525 binary HPLC pump (THF as the mobile phase, flow rate of 1 mL/min) using Waters styragel HR2 and HR5E columns, and polystyrene standards. Thermogravimetric analysis (TGA) was performed with a TA Instruments model Q5000 TGA, from room temperature to 600 °C at 20 °C/min. All samples were dried under vacuum for 2 days before measurement. Differential scanning calorimetry (DSC) was conducted with a TA Instruments Q1000 DSC, from -10 to 120 °C at a rate of 10 °C/min. Transmission electron microscopy (TEM) was accomplished using a JEOL 1011 TEM, operated at 100 kV. The samples were prepared by casting a thin film of nanocomposite on carbon-coated copper TEM grids. Particles size distribution, on the base of the profile of randomly selected quasi-spherically shaped particles, has been obtained using the ImageJ program. Selected area electron diffraction patterns were also obtained. XRD (Geigerflex Rigaku2, $2\theta = 0-80^{\circ}$, step = 0.05, dwell (s) = 3) was used to obtain powder X-ray diffraction pattern spectra using Cu-K α radiation $(\lambda = 0.154 \text{ nm})$. Noise corrections were made by using MDI Jade 7 software. The morphology of the block copolymers and the nanocomposite in powder form (sputter coated on sample holder) were examined by SEM (Zeiss ultra 55). Magnetic properties of the nanocomposites were measured using a superconducting quantum interference device (SQUID) magnetometer from Quantum Design. All the measurements were done in powder form of the sample after vacuum drying. The temperature dependence of the magnetization was determined by zero field-cooled (ZFC) and field-cooled (FC) measurements. The ZFC curve was obtained by cooling down to 4 K at zero magnetic fields and then measuring the magnetization under a 500 Oe applied magnetic field upto 300 K. The corresponding FC curves were similarly obtained, except that this time the sample was cooled while applying a 500 Oe magnetic field. The magnetizations as a function of applied magnetic field were also studied at 100 K above the blocking temperature.

2.1.3. Cytotoxicity (MTS) Assay

To test the cytotoxicity of the nanoparticles, 4×10^3 per well of Hela cells in 96-well plates were incubated in 90 µL of RPMI medium without phenol red, supplemented with 10% FBS and 100 units/mL penicillin-streptomycin for 24 h. Then the cells were incubated with various amounts of nanoparticles (1 µg/mL, 10 µg/mL, 20 µg/mL, 50 µg/mL) for additional 20 h. Subsequently, 20 µL of CellTiter 96[®] AQueous One Solution reagent was added into each well, followed by further incubation for 4 h at 37 °C. The relative viability of the cells incubated with nanoparticles to untreated cells was determined by measuring the MTS-formazan absorbance on a Kinetic microplate reader (Spectra Max M5, Molecular Devices, Sunnyvale, CA, USA) at 490 nm with a subtraction of the absorbance of cell-free blank volume at 490 nm. The results from three individual experiments were averaged.

2.2. Synthesis of 3-(3,5-Dimethyl-1H-Pyrazol-1-yl)-2-Hydroxypropyl Bicyclo[2.2.1] Hept-5-Ene-2-Carboxylate (2)

Monomer 1 was prepared according to our previous published procedure [46]. Epoxy monomer 1 (0.23 g, 1.2 mmol) in DMF was added dropwise to a suspension of 3,5-dimethylpyrazole (0.107 g, 1.11 mmol) and anhydrous potassium carbonate (0.166 g, 1.2 mmol) in 10 mL of anhydrous DMF. The reaction was stirred at 100 °C for 9 h until the disappearance of starting materials (followed by TLC). It was then cooled to room temperature, the salt was filtered off, and the solvent was removed under reduced pressure. A wheatish creamy solid (0.15 g, 55% yield) was obtained after column chromatography (1:1 hexane:ethyl acetate on silica) followed by vacuum drying overnight. ¹H NMR (500 MHz, CDCl₃) δ: 6.14–6.03 (m, 1.5H, HC=CH), 5.87 (m, 0.5H, HC=CH), 5.74 (s, 1H-Py ring), 4.52 (b, 1H, -OH), 4.17-3.85 (m, 6H), 3.15 (s, 0.5H), 2.98-2.90 (m, 1H), 2.89-2.86 (m, 1H), 2.20-2.13 (m, 6H, 2 -CH₃ in Py ring), 1.88-1.84 (s, 1H), 1.69-1.19 (m, 3H). ¹³C NMR (125 MHz, CDCl₃) δ : 176.05, 174.54, (C=O exo and endo) 148.24, 139.80, 138.14, 137.96, 137.92, 135.64, 132.26, 105.12 (=C-CH=C), 69.24, 65.19, 65.17, 65.04, 64.97, 49.72, 46.67, 46.36, 45.80, 45.77, 43.26, 43.04, 42.53, 41.64, 30.45, 29.31, 13.43 (Py-CH₃), 10.95 (Py-CH₃) IR (neat): 3349.48 (b, -OH), 3025.81 (=C-H stretch), 2925.08, 1732.36 (vs., C=O), 1601.25 (-C=C- stretch),1553.78 (-C=N-), 1492.89, 1452.06, 1333.81, 1272.80, 1232.39, 1180.06, 1029.02, 906.84, 756.10, 620.99 (-C=C- bend), 540.10 cm⁻¹. Anal. calcd for C₁₆H₂₂N₂O₃: C, 66.18, H, 7.64. Found: C, 65.96, H, 7.65.

2.3. Synthesis of Diblock Copolymer 5 by ROMP of 3-(3,5-Dimethyl-1H-Pyrazol-1-yl)-2-Hydroxypropyl Bicyclo[2.2.1]Hept-5-Ene-2-Carboxylate (5)

ROMP of monomer 2 with Grubbs second generation catalyst 3 was performed as shown in Scheme 1. The glassware was dried and purged with vacuum and N₂ in a Schlenk line several times prior to conducting the polymerization reaction. A solution (0.2 M) of monomer 2 (120 mg, 4.13×10^{-4} M, 175 eq) was prepared in dry CH₂Cl₂ under N₂. The catalyst solution was prepared by dissolving the catalyst in anhydrous CH₂Cl₂ under N₂ in a glovebox. The catalyst solution (2 mg, 2.36×10^{-6} M in 0.5 mL CH₂Cl₂, 1 eq) was added to the reaction mixture and stirred for 8 h at 30 °C. A norbornene solution (38 mg, 4.13×10^{-4} M, 175 eq) was injected and stirred for another 9 h. The polymerization reaction mixture was terminated with excess ethyl vinyl ether (300 eq relative to catalyst) and stirred for another 1 h. The reaction mixture was then poured into cold methanol and stirred, purified, and dried under vacuum, yielding a flaky white solid in 72% yield. ¹H NMR (500 MHz, CDCl₃) δ : 5.82 (b, CH, Py ring), 5.35–5.22 (b, -HC=CH-), 4.17–3.85, 3.18, 2.96, 2.44, 2.23–2.19, 1.87–1.27(b).

2.4. Stabilized Magnetic Dispersions

Preparation of monodisperse maghemite nanoparticles within copolymer matrices was accomplished by our previously reported method [30] using cyclohexanone as solvent or others as required.

2.5. Micelles Stabilized Magnetic Nanoparticle Dispersions in Water

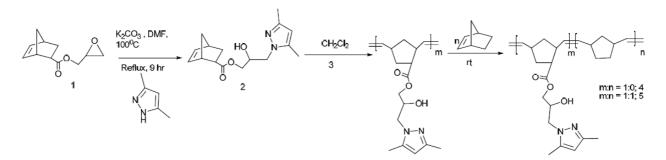
120 mg of F127 was dissolved in 20 mL (the concentration is higher than critical micelle concentrations (CMC); CMC of Pluronic F127 is 0.007 g/cm³ at room temperature) [36,38,39,47,48] of

water by vigorously stirring for 3 hrs. Maghemite-polymer nanocomposites (7 mg) were dispersed in CH_2Cl_2 . Equal volume of these two mixtures were added together and stirred under N_2 at 40 °C (waterbath) for until all CH_2Cl_2 evaporated in a fume hude and nanocomposite covered by the F127 coating was prepared in water. Then, it was subjected to centrifuge and finally, the light brown colored supernatant was collected which contains block copolymer-maghemite nanocomposites entrapped in pluronic micelles.

3. Results and Discussion

3.1. Synthesis of Monomer and Polymers

Scheme 1. Synthesis of monomers and block copolymers.



The monomer and polymers were designed and prepared by exploiting the versatility of epoxy precursor 1. In the first step, pyrazole-containing monomer 2 was synthesized from 1 [46], by opening the epoxide ring with 3,5-dimethyl pyrazole in the presence of base. Next, both a homopolymer 4 and a 1:1 diblock copolymer 5 were synthesized according to Scheme 1 via ROMP using Grubbs second generation catalyst (3, bis(tricyclohexylphosphine)-benzylideneruthenium dichloride). Copolymer 5 was prepared by sequential addition of monomer 2 and nobornene. The molecular weight and polydispersity of the polymers (Table 1) were controlled on the basis of a time-dependent study, monitoring monomer consumption by ¹H NMR and controlling the [M]/[I] ratio, where M is monomer and I is initiator.

The diblock copolymer template 5 contained the ligand system in one block that can chelate through both N-(from pyrazole) and O-donors (from ring-opened hydroxy and/or carboxylate groups) with the metal oxide core, while the second block contained the steric stabilizing group to disperse the nanoparticle composite and reduce interaction between nanoparticles. The pyrazole ligands played a vital role in stabilizing the maghemite nanoparticles, affording a supramolecular metal-organic hybrid. The polymers were characterized by ¹H NMR (Figure 1) and FTIR. In the ¹H NMR, distinct peaks at 6.14–5.87 ppm for -*CH*=*CH*- vinyl protons, 5.74 ppm for -*H* pyrazole ring and a broad -*OH* proton peak at 4.52 ppm were present for the monomer (Figure 1a) while the vinyl protons disappear and a new peak appears at 5.35–5.22 ppm for new alkene protons for the polymers Figure 1(b,c). The ratio between the alkene proton *vs.* pyrazole ring proton present in polymer determined the block ratio (m:n). The molecular weights of the polymers were experimentally determined by standard GPC (Figure 2) method calibrated with PS standards correspond to apparent Mn values, shown in Table1. The relatively high polydispersity index of the copolymer is possibly due to the presence of heteroatom (N, O) in the pendant group functionality.

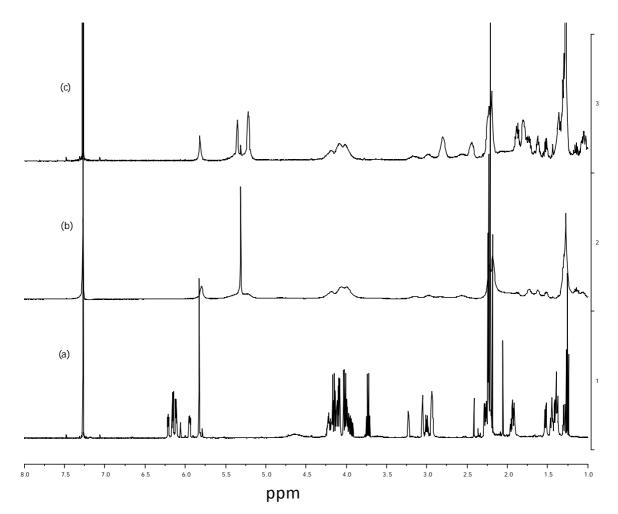
Block ratio (m:n)	M _n ^a (Theo)	m:n 1H NMR	M _n ^b (Exp)	PDI ^b	Block Ratio ^c	Tg (°C)	T ^d (°C)
200:0 (4)	58072	1:0	65085	1.42	224:0	46	170
175:175 (5)	67291	1.08:1	66331	1.33	176:163	39	217

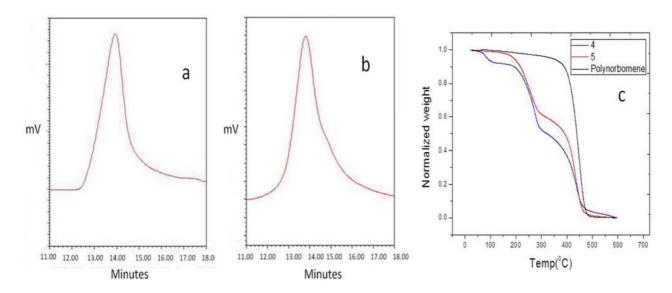
Table 1. Properties of the polymers.

^a: Theoretical molecular weight calculated from[M]/[I]feed; ^b: Mn and PDI were obtained experimentally from gel permeation chromatography (GPC) in THF relative to polystyrene standards; ^c: Actual polymer block ratio was calculated from the ¹H NMR and GPC results; ^d: Temperature at 10% weight loss.

The glass transition temperature and thermal decomposition temperature were determined by DSC and TGA analyses, respectively (Table 1). The 1:1 block copolymer 5 was more thermally stable (decomposition at 217 °C) compare to the pyrazole group containing homopolymer 4. Because of the thermally labile bond at the side chain, it was noticed, that the thermal stability of the polymer in general decreases with respect to homopolynorbornene (450 °C) or epoxy containing homopolymer (370 °C) as reported before [30]. The glass transition temperature of the polynorbornene, homopolymer, 4, and copolymer, 5 (were approximately 31, 46, and 39 °C respectively), were in close range and broad in nature.

Figure 1. ¹H NMR analysis supporting the formation of 1:1 diblock copolymer; (a) monomer 3; (b) homopolymer 4; and (c) 1:1 diblock copolymer 5.





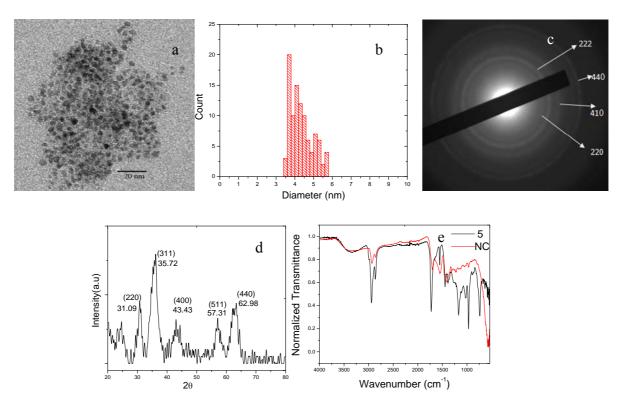
3.2. Synthesis and Characterization of Polymeric-Iron Oxide Nanocomposite

The second step was to generate relatively uniform, highly crystalline maghemite nanoparticles *in situ* from Fe(CO)₅ precursor in the presence of diblock copolymer 5 (0.68% molar wt of polymer compared to ironpentacarbonyl feed) in cyclohexanone. Supported by our previous study [31], 1:1 block copolymer ratio of the polymer was chosen to stabilize the nanopartcle stabilization at the optimum level. Trimethylamine N-oxide was used as an oxidizer to prepare the maghemite nanocomposite in a similar manner to our previously reported method [30,31]. Briefly, the block copolymer and iron-pentacarbonyl were added in cyclohexanone and refluxed under inert atmosphere until the solution turned to black. Thereafter, solution was cooled to room temperature and oxidizer was added to it, followed by reflux for another few hours, and then, purified as mentioned in literature. Finally, the nanocomposite was dispersed in solvent as required.

The block copolymer-stabilized nanocomposites were characterized by TEM, SEM, XRD, and FTIR. TEM (Figure 3a) confirmed generation of relatively uniform and spherical iron oxide nanoparticles. The size distribution (Figure 3b) of the nanoparticles was in the 3–6 nm range with an average size of 4.3 nm. Evidence of formation of a crystalline structure of the Fe₂O₃ nanoparticles was obtained by SAED and XRD (Figure 3(c,d)), revealing cubic maghemite-C type structures of the nanoparticles, corresponding well with standard data [49]. The average diameter (*d*) of the singular γ -Fe₂O₃ nanocrystallites, estimated using the Scherrer equation [50], was 4 nm, corresponding to the strongest reflection (311) of Fe₂O₃ nanoparticles at 2 θ value of 35.72°. This was in good agreement with TEM results. SEM data revealed the bulk morphology of the 1:1 block copolymer and nanocomposite. FTIR spectroscopic analysis provided compelling evidence of ligand-mediated binding of iron oxide with the pendant chelating group of the diblock copolymer (Figure 3e). The presence of a single, broad band at about 574 cm⁻¹ in the FTIR spectrum of the nanocomposite is characteristic of Fe-O stretching for less than 8 nm nanoparticles [51]. Also, the shift from 1732 cm⁻¹

to 1690 cm^{-1} , corresponding to C=O stretching in the polymer and nanocomposite, respectively, supported interaction between the iron oxide core and the diblock copolymer.

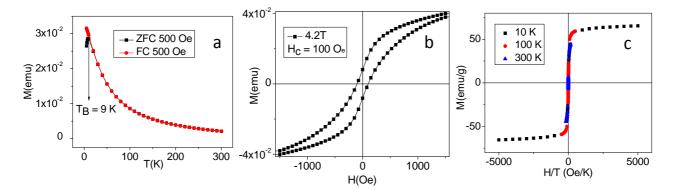
Figure 3. (a) TEM images of magnetic nanocomposite; (b) TEM nanoparticle size distribution histogram; (c) electron diffraction pattern of nanocomposite; (d) XRD analysis showing the presence of crystalline maghemite-C (NC-2); (e) FTIR analysis of 1:1 block copolymer (labeled 5) and magnetic nanocomposite (labeled NC).



3.3. Magnetic Properties of Nanocomposite

Magnetization (M) measurement as a function of temperature (T) was performed on γ -Fe₂O₃-diblock copolymer nanocomposites in powder form using SQUID. Figure 4a shows the zero field cooled (ZFC) and field cooled (FC) *vs.* temperature profile, where the blocking temperature (T_B) of 9 K is denoted by the peak of the ZFC curve. The low and sharp blocking temperature of the nanocomposite is consistent with the small and uniform size of the maghemite nanoparticles, respectively. Uniform distribution of the magnetic nanoparticles within the polymer matrix is further strengthened by very close superimposition of the ZFC and FC curves after passing the T_B. The magnetic hysteresis loop at 4.2 K, below T_B, is shown in Figure 4b. The coercive field was of the order of 100 Oe. Above T_B the coercive field was zero and the data collapse onto the same curve when plotted as a function of H/T. This H/T scaling behavior indicates that the sample consists of non-interacting superparamagnetic particles. The magnetization data above T_B are fit to a Langevin function, and a saturated moment of approximately 73 emu/g is determined from the fit.

Figure 4. (a) magnetization (M) *vs.* temperature (T) of the nanocomposite at 500 Oe applied magnetic field (H); (b) M-H loop below T_B shows coercive field (H_c) of 100 Oe; (c) M-H loop above T_B , coercive field (H_c) is zero.



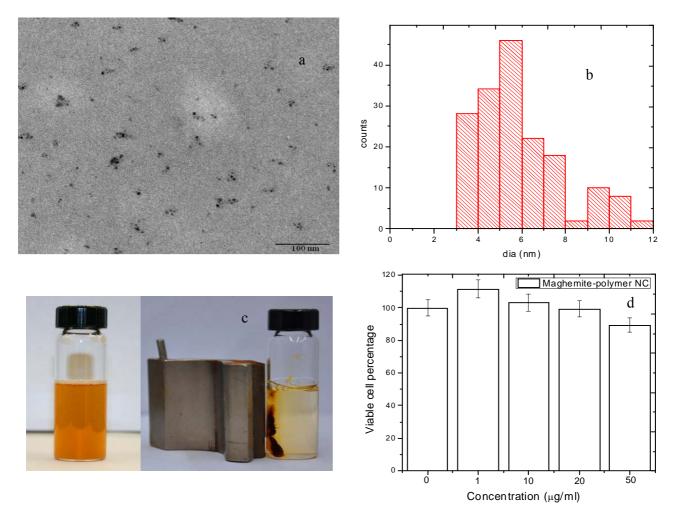
3.4. Formation of Biocompatible Nanocomposite

For potential biomedical applications, the stable dispersion in aqueous and physiological media, and biocompatibility of the pyrazole-containing block copolymer-stabilized maghemite nanocomposites was assessed. The organic soluble maghemite-polymer nanocomposites were dispersed in water using Pluoronic F127 (PEO-PPO-PEO), using to a solvent evaporation method. The Pluronic-coated, water-dispersible nanocomposite was generated by mixing an equal volume of the nanocomposite in CH₂Cl₂ with an aqueous solution of Pluronic F127, followed by vigorous stirring and evaporation of the CH₂Cl₂. The outer hydrophilic (PEO) blocks of Pluronic F127 help to form micelles and dispersion in water while the hydrophobic block (PPO) attracts the polymer-coated maghemite nanoparticles. An aqueous dispersion of micelle-encapsulated superparamagnetic nanocomposites was stable for weeks and retained their magnetic properties.

The morphology of the Pluronic-pyrazole-maghemite nanocomposites in water was studied by TEM (Figure 5a and 5b), indicating that the size of the core maghemite nanoparticles was similar before and after dispersion in water (confirming that the particles were stable and did not aggregate). The observed stability of the Pluronic-coated magnetic nanocomposites in water is important for biological use and was consistent to literature reports [45,52].

For potential biomedical applications, the cytotoxicity of PluronicTM-pyrazole block copolymer-coated superparamagnetic nanoparticles was assessed using a cell viability assay with Hela cells. Hela cells were incubated for 20 h with varying concentrations of the nanocomposites (0–50 μ M), exhibiting high cell viability, 90–100%, depending on concentration. Qin *et al.* reported a novel type ferrogel (SPIONS coated with oleic acid and PF127) to release drug for magnetically controlled release of hydrophobic drug very efficiently [42]. Recently, Zhao *et al.* also demonstrated a RGD modified ferrogel, where of SPION is encapsulated in PF127, alginate and AAD, for sustain release of cells and other bioactive agents under magnetic field [53]. Thus, the Pluronic encapsulated pyrazole block copolymer stabilized iron oxide nanocomposite also provides a promising tool to encapsulate hydrophobic drug or optical contrast agent and holds the potential for dual imaging modalities or theranostic applications in biomedical field.

Figure 5. (a) TEM image of Pluronic 127-coated polymer-maghemite nanocomposites; (b) TEM nanoparticle size distribution histogram; (c) photograph of Pluronic 127-stabilized polymer-Fe₂O₃ nanocomposite without (left) and with external applied magnetic field (right); and (d) cell viability of Pluronic 127-stabilized polymer-Fe₂O₃ nanocomposite incubated in Hela cells for 20 h as a function of concentration.



4. Conclusions

In summary, it is clear that well-defined *N*,*N*-dimethyl pyrazole-functionalized norbornene-based diblock copolymers are effective in stabilizing *in situ*-generated maghemite nanoparticles. The resulting nanocomposite exhibited strong superparamagnetism in the presence of an external magnetic field. Nanoparticle agglomeration was prevented through specific binding between the pendant ligands in the anchoring block and the iron oxide metal core. This organic block copolymer-inorganic maghemite nanocomposite underwent dynamic changes in magnetic properties and directional motion in response to an external magnetic field without destroying the integrity of the system. Pluronic127-coated magnetic nanocomposites were stable in aqueous media and possessed low cytotoxicity, making them potential candidates as contrast agents for MRI imaging, a carrier for drug delivery, or for use in magnetically-actuated biomimetic devices, subjects of future investigation.

Acknowledgements

We wish to acknowledge the National Science Foundation (CHE-0832622, and DMR-0704240) for support of this work.

References

- 1. Berry, C.C.; Curtis, A.S.G. Functionalisation of magnetic nanoparticles for applications in biomedicine. *J. Phys. D Appl. Phys.* **2003**, *36*, 198–206.
- 2. Pankhurst, Q.A.; Connolly, J.; Jones, S.K.; Dobson, J. Applications of magnetic particles in biomedicine. J. Phys. D Appl. Phys. 2003, 36, 167–181.
- 3. Chertok, B.; Moffat, B.A.; David, A.E.; Yu, F.; Bergemann, C.; Ross, B.D.; Yang, V.C. Iron oxide nanoparticles as a drug delivery vehicle for MRI monitored magnetic targeting of brain tumors. *Biomaterials* **2008**, *29*, 487–496.
- 4. Gupta, A.K.; Naregalkar, R.R.; Vaidya, V.D.; Gupta, M. Recent advances on surface engineering of magnetic iron oxide nanoparticles and their biomedical applications. *Nanomedicine* **2007**, *2*, 23–29.
- 5. Sun, C.; Lee, J.S.H.; Zhang, M. Magnetic nanoparticles in MR imaging and drug delivery. *Adv. Drug Delivery Rev.* **2008**, *60*, 1252–1265.
- 6. Shubayev, V.I.; Pisanic, T.R.; Jin, S. Magnetic nanoparticles for theragnostics. *Adv. Drug Delivery Rev.* **2009**, *61*, 467–477.
- 7. Oh, J.K.; Park, J.M. Iron oxide-based superparamagnetic polymeric nanomaterials: Design, preparation, and biomedical application. *Prog. Polym. Sci.* **2011**, *36*, 168–189.
- 8. Xulu, P.M.; Filipcsei, G.; Zrinyi, M. Preparation and responsive properties of magnetically soft poly(N-isopropylacrylamide) gels. *Macromolecules* **2000**, *33*, 1716–1719.
- 9. Csetneki, I.; Filipcsei, G.; Zrínyi, M. Smart nanocomposite polymer membranes with on/off switching control. *Macromolecules* **2006**, *39*, 1939–1942.
- 10. Filipcsei, G.; Csetneki, I.; Szilágyi, A.; Zrínyi, M. Magnetic field-responsive smart polymer composites. *Adv. Polym. Sci.* 2007, 206, 137–189.
- Zhang, L.; Abbott, J.J.; Dong, L.; Peyer, K.E.; Kratochvil, B.E.; Zhang, H.; Bergeles, C.; Nelson, B.J. Characterizing the swimming properties of artificial bacterial flagella. *Nano Lett.* 2009, *9*, 3663–3667.
- Fahrni, F.; Prins, M.W.J.; van Ijzendoorn, L.J. Magnetization and actuation of polymeric microstructures with magnetic nanoparticles for application in microfluidics. *J. Magn. Magn. Mater.* 2009, 321, 1843–1850.
- 13. Weissleder, R.; Pittet, M.J. Review article imaging in the era of molecular oncology. *Nature* **2008**, *452*, 580–589.
- Na, H.B.; Song, I.C.; Hyeon, T. Inorganic nanoparticles for MRI contrast agents. *Adv. Mater.* 2009, *21*, 2133–2148.
- 15. Shen, L.; Laibinis, P.E.; Hatton, T.A. Bilayer surfactant stabilized magnetic fluids: Synthesis and interactions at interfaces. *Langmuir* **1999**, *15*, 447–453.

- Kohler, N.; Sun, C.; Fichtenholtz, A.; Gunn, J.; Fang, C.; Zhang, M. Methotrexate-immobilized poly(ethylene glycol) magnetic nanoparticles for MR imaging and drug delivery. *Small* 2006, *2*, 785–792.
- Harisinghani, M.G.; Barentsz, J.; Hahn, P.F.; Deserno, W.M.; Tabatabaei, S.; van de Kaa, C.H.; de la Rosette, J.; Weissleder, R. Noninvasive detection of clinically occult lymph-node metastases in prostate cancer. *N. Engl. J. Med.* 2003, *348*, 2491–2499.
- Nasongkla, N.; Bey, E.; Ren, J.; Ai, H.; Khemtong, C.; Guthi, J.S.; Chin, S.F.; Sherry, A.D.; Boothman, D.A.; Gao, J. Multifunctional polymeric micelles as cancer-targeted, MRI-ultrasensitive drug delivery systems. *Nano Lett.* 2006, *6*, 2427–2430.
- 19. Raynal, I.; Prigent, P. ; Peyramaure, S.; Najid, A.; Rebuzzi, C.; Corot, C. Macrophage endocytosis of superparamagnetic iron oxide nanoparticles: Mechanisms and comparison of ferumoxides and ferumoxtran-10. *Invest. Radiol.* **2004**, *39*, 56–63.
- Sun, C.; Veiseh, O.; Gunn, J.; Fang, C.; Hansen, S.; Lee, D.; Sze, R.; Ellenbogen, R.G.; Olson, J.; Zhang, M. *In vivo* MRI detection of gliomas by chlorotoxin-conjugated superparamagnetic nanoprobes. *Small* 2008, *4*, 372–379.
- 21. Brazel, C.S. Magnetothermally-responsive nanomaterials: Combining magnetic nanostructures and thermally-sensitive polymers for triggered drug release. *Pharm. Res.* **2009**, *26*, 644–656.
- 22. Mouli, S.K.; Zhao, L.C.; Omary, R.A.; Thaxton, C.S. Lymphotropic nanoparticle enhanced MRI for the staging of genitourinary tumors. *Nat. Rev. Urol.* **2010**, *7*, 84–93.
- Will, O.; Purkayastha, S.; Chan, C.; Athanasiou, T.; Darzi, A.W.; Gedroyc, W.; Tekkis, P.P. Diagnostic precision of nanoparticle-enhanced MRI for lymph-node metastases: A meta-analysis. *Lancet Oncology* 2006, 7, 52–60.
- Neuwelt, E.A.; Hamilton, B.E.; Varallyay, C.G.; Rooney, W.R.; Edelman, R.D.; Jacobs, P.M.; Watnick, S.G. Ultrasmall superparamagnetic iron oxides (USPIOs): A future alternative magnetic resonance (MR) contrast agent for patients at risk for nephrogenic systemic fibrosis (NSF)? *Kidney Int.* 2009, 75, 465–474.
- Vellinga, M.M.; Engberink, O.; Raoul, D.; Seewann, A.; Pouwels, P.J.W.; Wattjes, M.P.; van der Pol, S.; Pering, C.; Polman, C.H.; de Vries, H.E. Pluriformity of inflammation in multiple sclerosis shown by ultra-small iron oxide particle enhancement. *Brain* 2008, *131*, 800–807.
- 26. Corot, C.; Robert, P.; Idée, J.M.; Port, M. Recent advances in iron oxide nanocrystal technology for medical imaging. *Adv. Drug Delivery Rev.* **2006**, *58*, 1471–1504.
- Lee, H.Y.; Lee, S.H.; Xu, C.; Xie, J.; Lee, J.H.; Wu, B.; Leen Koh, A.; Wang, X.; Sinclair, R.; Wang, S.X. Synthesis and characterization of PVP-coated large core iron oxide nanoparticles as an MRI contrast agent. *Nanotechnology* 2008, *19*, 165101:1–165101:6.
- Tang, T.Y.; Howarth, S.P.S.; Miller, S.R.; Graves, M.J.; Patterson, A.J.; U-King-Im, J.M.; Li, Z.Y.; Walsh, S.R.; Brown, A.P.; Kirkpatrick, P.J. The ATHEROMA (atorvastatin therapy: Effects on reduction of macrophage activity) study. Evaluation using ultrasmall superparamagnetic iron oxide-enhanced magnetic resonance imaging in carotid disease. *J. Am. Coll. Cardiol.* 2009, *53*, 2039–2050.
- Warren, S.C.; Messina, L.C.; Slaughter, L.S.; Kamperman, M.; Zhou, Q.; Gruner, S.M.; DiSalvo, F.J.; Wiesner, U. Ordered mesoporous materials from metal nanoparticle—block copolymer self-assembly. *Science* 2008, *320*, 1748–1752.

- 30. Biswas, S.; Belfield, K.D.; Das, R.K.; Ghosh, S.; Hebard, A.F. Block copolymer-mediated formation of superparamagnetic nanocomposites. *Chem. Mater.* **2009**, *21*, 5644–5653.
- Belfield, K.D.; Zhang, L. Norbornene-functionalized diblock copolymers via ring-opening metathesis polymerization for magnetic nanoparticle stabilization. *Chem. Mater.* 2006, 18, 5929–5936.
- Anderson, B.F.; Baker, H.M.; Norris, G.E.; Rice, D.W.; Baker, E.N. Structure of human lactoferrin: Crystallographic structure analysis and refinement at 2.8 A resolution. *J. Mol. Biol.* 1989, 209, 711–734.
- 33. James, N.G.; Berger, C.L.; Byrne, S.L.; Smith, V.C.; MacGillivray, R.T.A.; Mason, A.B. Excited-state lifetime studies of the three tryptophan residues in the N-lobe of human serum transferrin. *Biochemistry* **2007**, *46*, 10603–10611.
- Bielawski, C.W.; Grubbs, R.H. Living ring-opening metathesis polymerization. *Prog. Polym. Sci.* 2007, 32, 1–29.
- 35. Buchmeiser, M.R. *Handbook of Ring-Opening Polymerization*, 1st ed; Dubois, P., Coulemibier, O., Raquez, J.M., Eds.; Wiley-VCH: Berlin, Germany, 2009.
- 36. Hilf, S.; Kilbinger, A.F.M. Functional end groups for polymers prepared using ring-opening metathesis polymerization. *Nat. Chem.* **2009**, *1*, 537–546.
- Merrett, K.; Liu, W.; Mitra, D.; Camm, K.D.; McLaughlin, C.R.; Liu, Y.; Watsky, M.A.; Li, F.; Griffith, M.; Fogg, D.E. Synthetic neoglycopolymer-recombinant human collagen hybrids as biomimetic crosslinking agents in corneal tissue engineering. *Biomaterials* 2009, *30*, 5403–5408.
- 38. Kabanov, A.V.; Batrakova, E.V.; Alakhov, V.Y. Pluronic block copolymers as novel polymer therapeutics for drug and gene delivery. *J. Control. Release* **2002**, *82*, 189–212.
- 39. Moghimi, S.M. Mechanisms regulating body distribution of nanospheres conditioned with pluronic and tetronic block co-polymers. *Adv. Drug Delivery Rev.* **1995**, *16*, 183–193.
- 40. Wadhwa, S.; Paliwal, R.; Paliwal, S.R.; Vyas, S.P. Nanocarriers in ocular drug delivery: An update review. *Curr. Pharm. Des.* **2009**, *15*, 2724–2750.
- 41. Lim, J.K.; Majetich, S.A.; Tilton, R.D. Stabilization of superparamagnetic iron oxide core-gold shell nanoparticles in high ionic strength media. *Langmuir* **2009**, *25*, 13384–13393.
- 42. Qin, J.; Asempah, I.; Laurent, S.; Fornara, A.; Muller, R.N.; Muhammed, M. Injectable superparamagnetic ferrogels for controlled release of hydrophobic drugs. *Adv. Mater.* **2009**, *21*, 1354–1357.
- 43. Gonzales, M.; Krishnan, K.M. Phase transfer of highly monodisperse iron oxide nanocrystals with Pluronic F127 for biomedical applications. *J. Magn. Magn. Mater.* **2007**, *311*, 59–62.
- 44. Lin, J.J.; Chen, J.S.; Huang, S.J.; Ko, J.H.; Wang, Y.M.; Chen, T.L.; Wang, L.F. Folic acid-Pluronic F127 magnetic nanoparticle clusters for combined targeting, diagnosis, and therapy applications. *Biomaterials* **2009**, *30*, 5114–5124.
- 45. Morales, M.A.; Jain, T.K.; Labhasetwar, V.; Leslie-Pelecky, D.L. Magnetic studies of iron oxide nanoparticles coated with oleic acid and Pluronic block copolymer. *J. Appl. Phys.* **2005**, *97*, 10Q905:1–10Q905:3.
- 46. Biswas, S.; Belfield, K.D. Self-assembled block copolymer/superparamagnetic nanoparticle nanocomposites. *Polym. Prepr. Am. Chem. Soc. Div. Polym. Chem.* **2008**, *49*, 1063–1064.

- 47. Bohorquez, M.; Koch, C.; Trygstad, T.; Pandit, N. A study of the temperature-dependent micellization of pluronic F127. *J. Colloid Interface Sci.* **1999**, *216*, 34–40.
- 48. Sakai, T.; Alexandridis, P. Mechanism of gold metal ion reduction, nanoparticle growth and size control in aqueous amphiphilic block copolymer solutions at ambient conditions. *J. Phys. Chem. B* **2005**, *109*, 7766–7777.
- 49. MDI Jade, version 7; MDI: Livermore, CA, USA, 2009; PDF No. 00-039-1346.
- 50. Xia, H.; Foo, P.; Yi, J. Water-dispersible spherically hollow clusters of magnetic nanoparticles. *Chem. Mater.* **2009**, *21*, 2442–2451.
- Li, D.; Teoh, W.Y.; Selomulya, C.; Woodward, R.C.; Munroe, P.; Amal, R. Insight into microstructural and magnetic properties of flame-made γ-Fe₂O₃ nanoparticles. *J. Mater. Chem.* 2007, 17, 4876–4884.
- Jain, T.K.; Reddy, M.K.; Morales, M.A.; Leslie-Pelecky, D.L.; Labhasetwar, V. Biodistribution, clearance, and biocompatibility of iron oxide magnetic nanoparticles in rats. *Mol. Pharm.* 2008, *5*, 316–327.
- 53. Zhao, X.; Kim, J.; Cezar, C.A.; Huebsch, N.; Lee, K.; Bouhadir, K.; Mooney, D.J. Active scaffolds for on-demand drug and cell delivery. *Proc. Natl. Acad. Sci.* **2011**, *108*, 67–72.

 \bigcirc 2012 by the authors; licensee MDPI, Basel, Switzerland. This article is an open access article distributed under the terms and conditions of the Creative Commons Attribution license (http://creativecommons.org/licenses/by/3.0/).